RSC Advances

PAPER

View Article Online
View Journal | View Issue

Cite this: *RSC Adv.*, 2025, **15**, 24381

An isophorone-derived AIE-active probe for peroxynitrite detection and bioimaging applications†

Raguraman Lalitha,[a] Vishnu Halnor Vivek,[a] Yueh-Hsun Lu,[b] Shu Pao Wu[b] and Sivan Velmathi *[a]

Received 29th March 2025
Accepted 19th June 2025

DOI: 10.1039/d5ra02185e

rsc.li/rsc-advances

Compounds exhibiting aggregation-induced emission (AIE) are remarkable due to their characteristic restriction of intramolecular rotation, making them highly versatile for a wide range of applications. Herein, an isophorone based probe (IHP) was developed for the detection of peroxynitrite ($ONOO^-$) using the C=N as the reactive group. Photophysical investigations were conducted to explore the aggregation behaviour of IHP in two different solvent systems: DMSO:PBS and DMSO. In DMSO, only the monomeric form of the dye was observed, showing no unusual behaviour. However, in DMSO : PBS (1 : 1), multiple emitting species were detected, indicating the coexistence of dye aggregates and monomers. The fluorescence spectra exhibited wavelength-dependent changes, with the aggregates displaying a red-shift compared to the monomers, indicating J-aggregation. The AIE properties of IHP resulted in red emission, with a fluorescence response towards $ONOO^-$ through oxidative cleavage of the C=N bond to an aldehyde accompanied by the shift in emission maximum. Under physiological conditions, the probe exhibited good selectivity and high sensitivity to $ONOO^-$, low detection limit of 1.1 μM and rapid recognition within 200 seconds. Furthermore, the probe was effectively used to image exogenous and endogenous peroxynitrite in living cells.

1. Introduction

Nitric oxide (NO) is converted into intracellular reactive nitrogen species (RNS) by electron transfer reactions.[1,2] Peroxynitrite ($ONOO^-$), a RNS produced by the reaction of nitric oxide (NO) and superoxide anion radicals ($O_2^{-\bullet}$).[3] This substance is produced in mitochondria and is important for cell signal transduction, stress response and antibacterial activity.[4] Elevated levels of $ONOO^-$ can damage vital cellular components, and may contribute to the development of various diseases,[5–7] including inflammation, circulatory shock, cancer, diabetes *etc.*[8,9] At a pH of 7.4, $ONOO^-$ shows higher reactivity towards a wide range of bioactive substances, including proteins and lipids, exhibiting exceptionally high reactivity levels.[8,10–12] Besides its inherent oxidation, nucleophilic, and nitration properties, $ONOO^-$ has the capability to transform into more potent secondary free radicals, such as nitro radicals ($NO_2^\bullet$), hydroxyl radicals ($OH^\bullet$), and carbonate radicals ($CO_3^{-\bullet}$). These secondary radicals subsequently interact with biomolecules, and ultimately cause cell death.[13,14] Therefore, it is crucial to establish an accurate approach for $ONOO^-$ detection in living cells.

The use of small organic fluorescent probes has become an effective method for identifying species that are physiologically active within living systems, providing high temporal resolution.[12,15–18] Their affordability, along with their notable attributes such as high selectivity, sensitivity, and easy monitoring, has garnered significant attention from numerous researchers.[19] Nevertheless, certain drawbacks are linked to these conventional fluorescent sensors. They are highly fluorescent in the molecular state but weakly fluorescent or non-emissive in the aggregated state, leading to aggregation-caused quenching (ACQ), which adversely affects their sensing capabilities.[20,21] Moreover, highly polar solvents exert a considerable impact on the fluorescence intensity and stability of certain fluorescent compounds.[22] As a result, the design of fluorescent sensors that exhibit remarkable durability in polar solvents and high fluorescence in an aggregated state has gained growing importance. In dye chemistry, self-association, or aggregation, of dyes in solution or at solid–liquid interfaces is a common phenomenon due to the intermolecular van der Waals attractive forces between dye molecules.[23–26]

In recent years, fluorogens with a unique feature known as aggregation-induced emission (AIE) have become an emergent category of fluorescent sensors. The AIE fluorogens typically

---

[a] *Organic and Polymer Synthesis Laboratory, Department of Chemistry, National Institute of Technology, Tiruchirappalli – 620 015, India. E-mail: velmathis@nitt.edu*
[b] *Department of Applied Chemistry, National Yang Ming Chiao Tung University, Hsinchu 30010, Republic of China*

† Electronic supplementary information (ESI) available. See DOI: https://doi.org/10.1039/d5ra02185e

exhibit little to no emission when dissolved at the molecular level but exhibit strong emission when they aggregate into larger molecular clusters, operating through a mechanism of restriction of intramolecular motions (RIMs).[19,27–29] Primarily, various molecular interactions, such as steric effects, hydrogen bonding inhibit intramolecular rotations favouring a radiative pathway, leading to strong fluorescence emission. This phenomenon enhances the potential for on-site sensing using a AIE fluorophore. Furthermore, the AIE phenomenon offers numerous advantages to AIE based sensors including reduced background noise, a large Stoke's shift, and enhanced signal amplification which is ideal for biosensing and bioimaging.[19,27–29] These appealing photophysical properties have prompted researchers to develop numerous AIE-active fluorescent molecules. These molecules are being utilized in numerous applications, such as optoelectronic devices, biosensors, and the detection of explosives and metal ions.[30–34]

There are few AIE probes reported in the literature for $ONOO^{-\bullet}$,[35–43] nevertheless, developing AIE-active fluorescent probes for the efficient detection of $ONOO^-$ remains essential due to the significant role this analyte plays in both biological and chemical fields. While numerous fluorescent probes have been reported for the detection of $ONOO^-$,[44–48] many of these probes suffer from slow response times, which is not suitable for peroxynitrite detection due to the short lifetime of $ONOO^-$ under physiological conditions and operate in the short-wavelength window (<600 nm) (Table S1†), thus leading to low signal-to-background ratio and poor accuracy of imaging limiting their biological applications.

In this work, we developed an isophorone derivative, 2-(3-((*E*)-4-hydroxy-3-((*E*)-(2-(pyridin-2-yl)hydrazineylidene)methyl)styryl)-5,5-dimethylcyclohex-2-en-1-ylidene)malononitrile(IHP). The probe has hydrazinyl pyridine moiety which act as electron donor and the dicyanoisophorone moiety as the electron acceptor. This donor–acceptor groups can render the molecule to Intramolecular Charge Transfer (ICT) behaviour. A systematic investigation of IHP's photophysical properties was conducted in different ratios of DMSO (good solvent) and PBS (a bad solvent) to explore its aggregation behaviour and the resulting changes in fluorescence properties. Notably, IHP contains a C=N moiety, which serves as a reactive site for oxidative cleavage by $ONOO^-$. The IHP probe exhibits a shift in emission maxima in response to $ONOO^-$, also demonstrated better analytical properties for detecting $ONOO^-$, including rapid response time, high sensitivity, and strong selectivity. Owing to these properties, IHP can function as a sensitive fluorescent sensor for $ONOO^-$, making it valuable for detecting this species in living cells through fluorescence microscopy.

2. Materials

2.1 Chemicals and instruments

All chemicals were sourced from commercial dealers and used as such. Silica gel with a mesh size of 100–200 was employed for column chromatography. Proton and carbon NMR were recorded on a Bruker AV-500 NMR spectrometer. An Agilent QTOF G6545 spectrometer with a resolution of 50 000 in electrospray ionization (ESI) mode was used to measure HRMS. Absorption spectra were recorded with a Shimadzu UV-2600 spectrophotometer, and emission spectra were obtained using a Shimadzu RF-5301PC fluorescence spectrophotometer. HeLa cells, a human cervical cancer cell line, were obtained from the Culture Collection and Research Center, Food Industry Research and Development Institute (FIRDI) in Hsinchu, Taiwan.

2.2 Synthesis of the sensing molecule

The synthesis procedure of compound **1–3** is given in ESI data† and their characteristic data is given in Fig. S1–S6.†

2.2.1 Synthesis of 2-(3-((*E*)-4-hydroxy-3-((*E*)-(2-(pyridin-2-yl)hydrazinylidene) methyl) styryl)-5,5-dimethylcyclohex-2-en-ylidene) malononitrile (IHP). The mixture of compound 3 (0.115 g, 0.36 mmol) and 2-hydrazinylpyridine (0.047 g, 0.43 mmol) in anhydrous ethanol (10 mL) was refluxed at 85 °C for six hours (Scheme 1). The reaction mixture was added drop by drop into cold water. The precipitate formed was filtered to

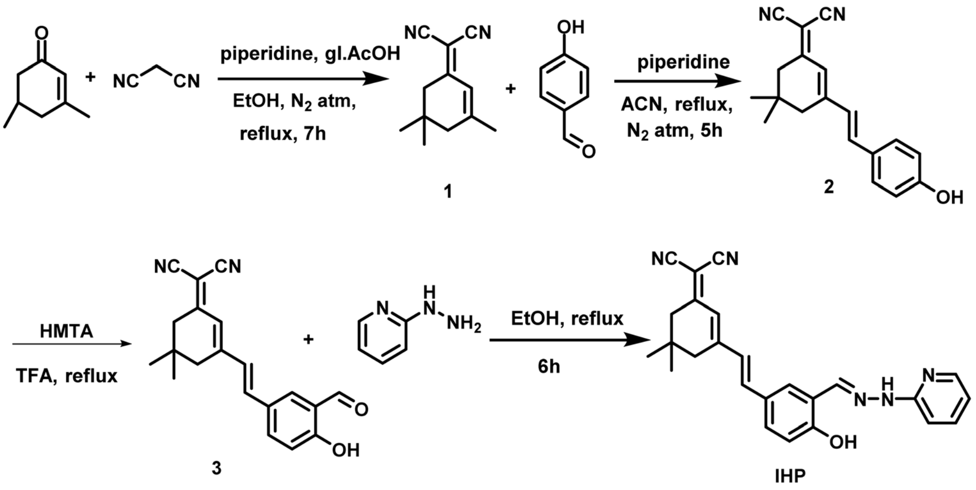

Scheme 1 Synthetic route of the probe IHP.

afford a brick red solid (yield = 0.12 g, 86%). Melting point 262–265 °C.

^{1}H NMR (500 MHz, DMSO-d_6) δ (ppm): 1.02 (s, 6H), 2.55 (s, 2H), 2.60 (s, 2H), 6.78–6.8 (m, 1H), 6.85 (s, 1H), 6.94 (d, J = 8.5 Hz, 1H), 7.14 (d, J = 8. Hz, 1H), 7.27 (d, J = 16 Hz, 1H), 7.30 (d, J = 16 Hz, 1H), 7.59–7.61 (m, 1H), 7.66–7.68 (m, 1H), 7.93 (d, J = 2.05 Hz, 1H), 8.14–8.15 (m, 1H), 8.28 (s, 1H), 10.96 (s, 1H), 11.0 (s, 1H).

^{13}C NMR (125 MHz, DMSO-d_6) δ (ppm): 27.4, 31.6, 38.2, 42.3, 75.1, 106.3, 113.2, 114.0, 115.1, 116.6, 121.1, 121.6, 127.0, 127.3, 127.6, 129.0, 137.4, 137.9, 147.8, 156.3, 156.5, 157.4, 170.2 (Fig. S7 and S8†).

HRMS (ESI, *m*/*z*): calculated $[C_{25}H_{24}N_5O]^+$, 410.1976; found 410.1984 (Fig. S9†).

2.3 Spectral acquisition

1 mM stock solution of IHP in DMSO and 10 mM of analyte solution in water was made. For absorption and emission studies 20 μM of IHP and 100 μM of analytes were added and diluted to 2 mL using DMSO : PBS (10 mM, pH 7.4, 1 : 1). For consistency, each sensing experiment was carried out three times at room temperature. Excitation wavelength 460 nm was used to record the fluorescence spectra.

2.4 Cytotoxicity assay

Using the conventional MTT (3-(4, 5-dimethylthiazol-2-yl)-2, 5-diphenyltetrazolium bromide) assay, the cytotoxicity of IHP towards the experimental cells was assessed. In summary, HeLa cells were cultured for one night in 96-well plates, and then for one day at 37 °C. The cells were exposed to several doses of IHP (0, 5, 10, 15, 20, 25 μM) after which the cells were treated with 50 μL of MTT solution (5 mg mL^{-1}) and incubated at 37 °C for an extra 4 hours. Following the extraction of the leftover MTT, 150 μL of DMSO was introduced into every well to dissolve the formazan crystals formed. The absorbance of each well at 570 nm was measured with a microplate reader. The cells showed 90% cell viability (Fig. S10†) which indicated that IHP is less toxic to the cells and can be used for bioimaging.

2.5 Cell imaging

HeLa cells were cultured in Dulbecco's Modified Eagle Medium (DMEM) supplemented with 10% fetal bovine serum (FBS) and 1% (v/v) antibiotic solution at 37 °C in incubator containing 5% CO_2. For imaging experiments, cells were seeded into 6-well plates and allowed to adhere for 24 hours. The culture medium was then replaced with fresh DMEM, and cells were incubated with the fluorescent probe IHP (10 μM) for 20 minutes. After incubation, the medium was removed, and cells were washed twice with phosphate-buffered saline (PBS) to remove probe.

Cells were then treated with peroxynitrite (ONOO$^-$, 100 μM) for 5 minutes. For the ONOO$^-$ scavenger group, cells were co-incubated with ONOO$^-$ (50 μM) and uric acid (200 μM) for 15 minutes. To stimulate endogenous ONOO$^-$ production, lipopolysaccharide (LPS, 1 μg mL^{-1}) and phorbol 12-myristate 13-acetate (PMA, 10 nM) were dissolved in DMEM and applied to the cells for 1 hour.

Following treatment, the medium was removed, and cells were washed twice with PBS. Nuclear staining was performed using 4′,6-diamidino-2-phenylindole (DAPI, 0.02 mg mL^{-1}) for 15 minutes at room temperature, followed by PBS washes to remove excess dye. The cells were fixed with 4% formaldehyde for 15 minutes. The coverslips were then mounted for confocal fluorescence imaging.

3. Results and discussion

3.1 Synthesis and design

The probe was synthesised by four steps as detailed above in the experimental section and characterised using NMR and HRMS. The NMR characterisation of probe and intermediates and the HRMS data of the probe is given in ESI (Fig. S1 to S9).† The probe IHP was designed for peroxynitrite detection, initially assumed to be non-emissive due to C═N isomerization. Upon oxidative cleavage of the C═N bond, it was expected to regenerate compound **3**, an Excited State Intramolecular Proton Transfer (ESIPT) emissive molecule.[49] However, IHP exhibited AIE behaviour, displaying red emission upon aggregation. Upon reaction with ONOO$^-$, the emission maximum shifted, corresponding to the formation of compound **3**.

3.2 Photophysical properties

UV-vis and fluorescence studies were conducted using 10 μM of IHP in different solvents varying from non-polar to polar solvents. The absorbance spectra showed two bands at approximately around 360 nm and 440 nm, and it was almost the same in all solvents, which implies that the absorption profiles are free from the effect of solvent polarity. In the emission spectra, IHP showed solvatochromic behaviour. The molecule IHP has the pyridinyl moiety as the donor group and the dicyanoisophorone moiety as the acceptor group. The lower energy absorption band corresponds to the n to π* transition of the pyridinyl moiety and the high energy absorption band corresponds to ICT transitions from the electron releasing pyridinyl moiety to the electron accepting isophorone moiety and the π to π* transition. There was shift in the emission maximum towards longer wavelength as we moved from non-polar to polar solvents (Fig. S11†). This can be attributed to the ICT effect of the molecule.

3.2.1 Aggregation induced emission studies. The AIE property of the probe was studied in binary solvent system consisting of different ratios of DMSO (good solvent) and 10 mM, PBS, pH 7.4 (bad solvent). IHP in DMSO showed two absorption peaks at 364 nm and 440 nm and as the PBS fraction increased up to 20%, there was only a slight change in the absorption maxima, and IHP was weakly emissive in DMSO because of the C═N isomerisation of the molecule which makes it non-emissive.

When the PBS buffer ratio was increased to 50% there was a red shift in absorption bands of IHP from 364 nm and 440 nm to 435 nm and 540 nm respectively, and the level off tails observed in the visible region (Fig. S12a†) shows the AIE behaviour of IHP.[30] This shift is likely attributed to the aggregation of IHP induced by this solvent mixture. Since aggregation is a process mediated by solvents, the behaviour of molecules during aggregation will be strongly influenced by the inherent hydrophilicity and hydrophobicity of both the solvents and the molecules involved. It's well-known that many organic compounds have the tendency to aggregate in poor solvents, including water.[19]

In the emission spectra, IHP was non-emissive in DMSO (good solvent), when the PBS (bad solvent) fraction increased to 50%, there was dramatic increase in the emission intensity (at 635 nm) with no shift in emission maxima, this dramatic increase can be attributed to the AIE behaviour of IHP, which was proved by the SEM analysis which shows spherical aggregates in 50% PBS (Fig. 1a). When the PBS fraction was greater than 50%, there was a new peak at 644 nm with reduced intensity which may be due to the formation of aggregates of different morphology[31] (Fig. S12b†). The SEM results taken in 90% PBS showed the formation of aggregates of different morphology which had flakelike structure (Fig. 1b). To ascertain that the aggregates contain the IHP molecule rather than components from the PBS buffer, elemental mapping was conducted. The results confirmed the presence of the IHP molecule within the aggregates, as illustrated in Fig. S13.†

The fluorescence lifetime was measured Fig. S14,† and the lifetime in DMSO (good solvent) was 0.02 ns, because there was minimal aggregation and the molecules are well-dispersed, the fluorescence intensity was low due to the intramolecular rotations leading to the non-radiative decay and hence the fluorescence lifetime is short as the non-radiative pathway dominates.

The fluorescence lifetime in DMSO : PBS (1 : 1), where the AIE effect was prominent was 0.06 ns. The lifetime is longer than in pure DMSO, reflecting the enhanced radiative pathway. The lifetime in 90% PBS is 0.057 ns, where there is slight decrease in the lifetime as compared to the emissive AIE form.

When fluorescence quenching is observed upon increasing the PBS fraction beyond 50%, it may result from the formation of large aggregates or agglomerates. These structures can facilitate non-radiative decay pathways, such as π–π stacking interactions or light scattering, leading to a significant decrease in fluorescence lifetime.

Conversely, if the quenching is primarily due to the IFE, where the sample itself absorbs excitation or emission light, the fluorescence lifetime typically remains unchanged, as IFE affects the intensity but not the excited-state deactivation pathways.[50–54]

Herein, the slight decrease in fluorescence lifetime from 0.06 ns in the DMSO : PBS (1 : 1) mixture to 0.057 ns in 90% PBS suggests that both aggregation-induced non-radiative decay and IFE contribute to the observed quenching. The minimal change in lifetime indicates that while aggregation introduces some non-radiative decay pathways, IFE plays a significant role in reducing fluorescence intensity without substantially affecting the lifetime.

Therefore, the observed fluorescence quenching at higher PBS concentrations is likely due to a combined effect of agglomerate formation and the inner filter effect.

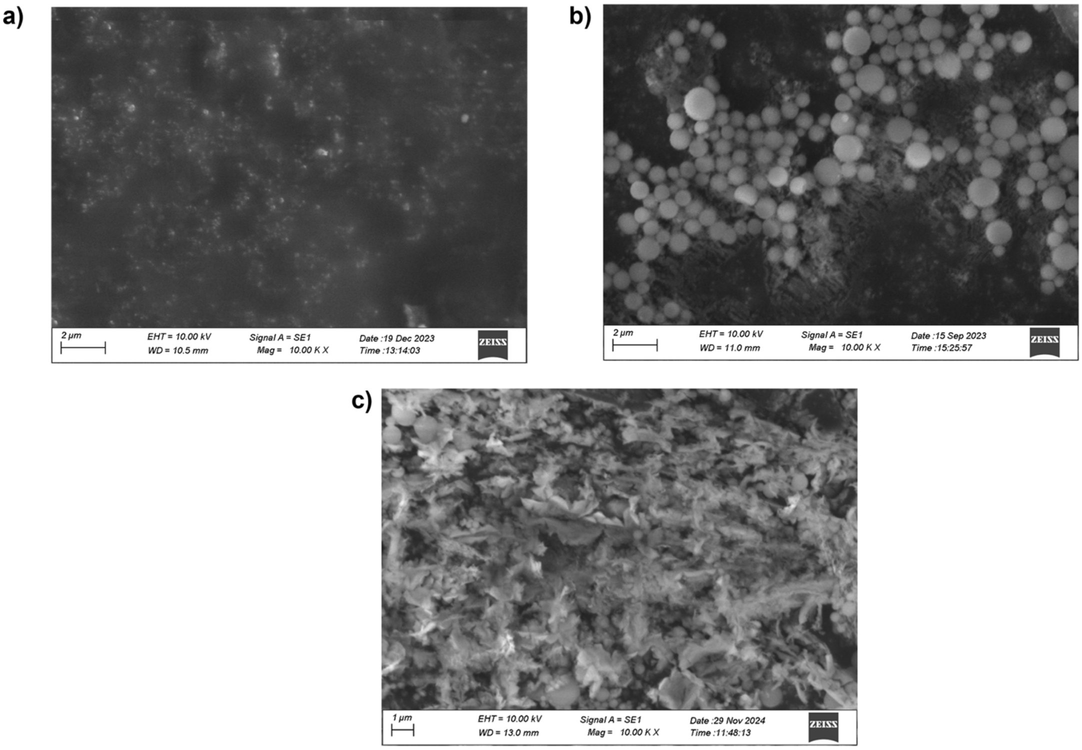

Fig. 1 (a) SEM image of IHP (10 μM) in DMSO (b) SEM image of IHP (10 μM) in DMSO : PBS (1 : 1, v/v, pH 7.4) (c) SEM image of IHP (10 μM) in DMSO : PBS (1 : 9, v/v, pH 7.4).

3.2.2 Excitation wavelength-dependent emission: confirmation of J-aggregates. The red shift in the absorption bands of IHP in DMSO : PBS (10 mM, pH 7.4 1 : 1) is explained by the Kasha's molecular exciton theory.[55] This theory put forward that an end-to-end alignment of chromophore transition dipoles, or J-aggregates, is allowed to transition from the ground state to a lower energy exciton state, which causes the bathochromic shift in the UV spectra (Fig. S15a†). In contrast, a face-to-face alignment of dipole moments, or H-aggregation, results in a hypsochromic shift, which signifies a transition to a higher energy exciton state. Thus, the observed shift in absorption of IHP indicates the formation of J-aggregates.[56,57] In DMSO solvent, there was no significant fluorescence emission of IHP. However, with increasing PBS fraction up to 50%, a red emission is observed with emission maximum at 635 nm (Fig. S15b†). Restrictions in intramolecular rotation, cause the emission intensity to increase and activate the radiative pathway, with a higher degree of aggregation at 50% PBS. This observation was supported by increase in quantum yield from 0.004 to 0.08 with the increase in PBS fraction from 0 to 50%.

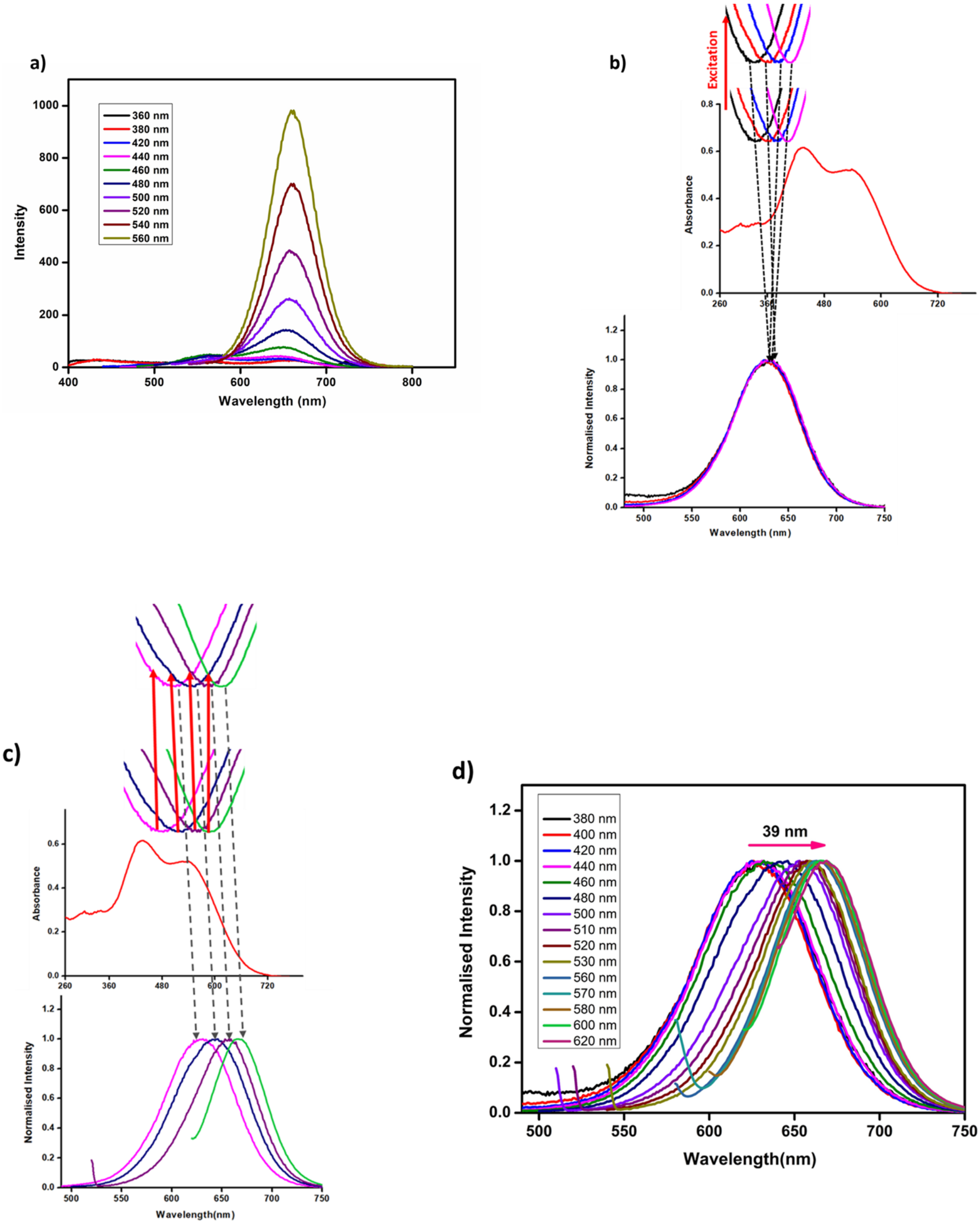

Fig. 2 (a) Emission spectra of IHP in DMSO at different excitation wavelengths (b) emission spectra of IHP in DMSO : PBS (1 : 1) excited at the blue edge of the absorption spectra (c) emission spectra of IHP in DMSO : PBS (1 : 1) excited at the red edge of the absorption spectra (d) normalised emission spectra of IHP in DMSO : PBS (1 : 1) excited at different excitation wavelengths.

In both DMSO and DMSO:PBS solutions, we examined the emission spectra of IHP throughout a range of excitation wavelengths that covered the red and blue margins of the absorption spectra. The emission spectra in DMSO obtained at various excitation wavelengths showed no discernible spectral changes. The emission maximum was at 656 nm even on exciting at various excitation wavelength (Fig. 2a). However, in DMSO:PBS, the difference in the emission spectra was notably low when the monitoring excitations were maintained at the blue edge of the spectrum (Fig. 2b), indicating emissions from monomeric species. Conversely, a bathochromic shift was seen in the emission maxima when the excitation wavelengths were situated at the red edge of the spectrum (Fig. 2c), known as the red-edge effect, which deviates from Kasha's rule. This red shift in emission peak, with a magnitude as large as 39 nm, persisted until a noise-free spectrum could be recorded (Fig. 2d),[58] suggesting the presence of multiple emitting species when IHP is dissolved in DMSO:PBS. These multiple species arise from aggregation, with the aggregates predominantly being strongly fluorescent J-aggregates. Since each aggregated species possesses its own fluorescence maxima, a change in the excitation wavelength results in the excitation of a different species and the observation of emission characteristic of that species. A 3D model directly representing the Excitation Emission Matrices (EEM) data in three dimensions, showing excitation wavelength, emission wavelength, and fluorescence intensity represented in Fig. S16† shows strong, red-shifted emissions, narrow peaks and relatively small Stoke's shift also proves the J-type behaviour of the aggregates.

To further validate the aggregation behaviour of IHP and ascertain whether the change in fluorescence was a result of aggregation or the presence of salts in the PBS buffer, emission spectra of IHP were conducted in different ratios of DMSO to H_2O. It was found that similar emission pattern was observed as it was in DMSO:PBS. The maximum emission intensity was observed in DMSO : H_2O (1 : 1) (Fig. S17†). On conducting the excitation-dependent emission experiments, there was red-edge effect observed even in DMSO:H_2O (Fig. 3a) but the magnitude of the red shift was less (29 nm) compared to the red-shift seen in DMSO:PBS (39 nm).

This led us to contemplate the factors influencing this change, and our focus turned to pH. Consequently, we

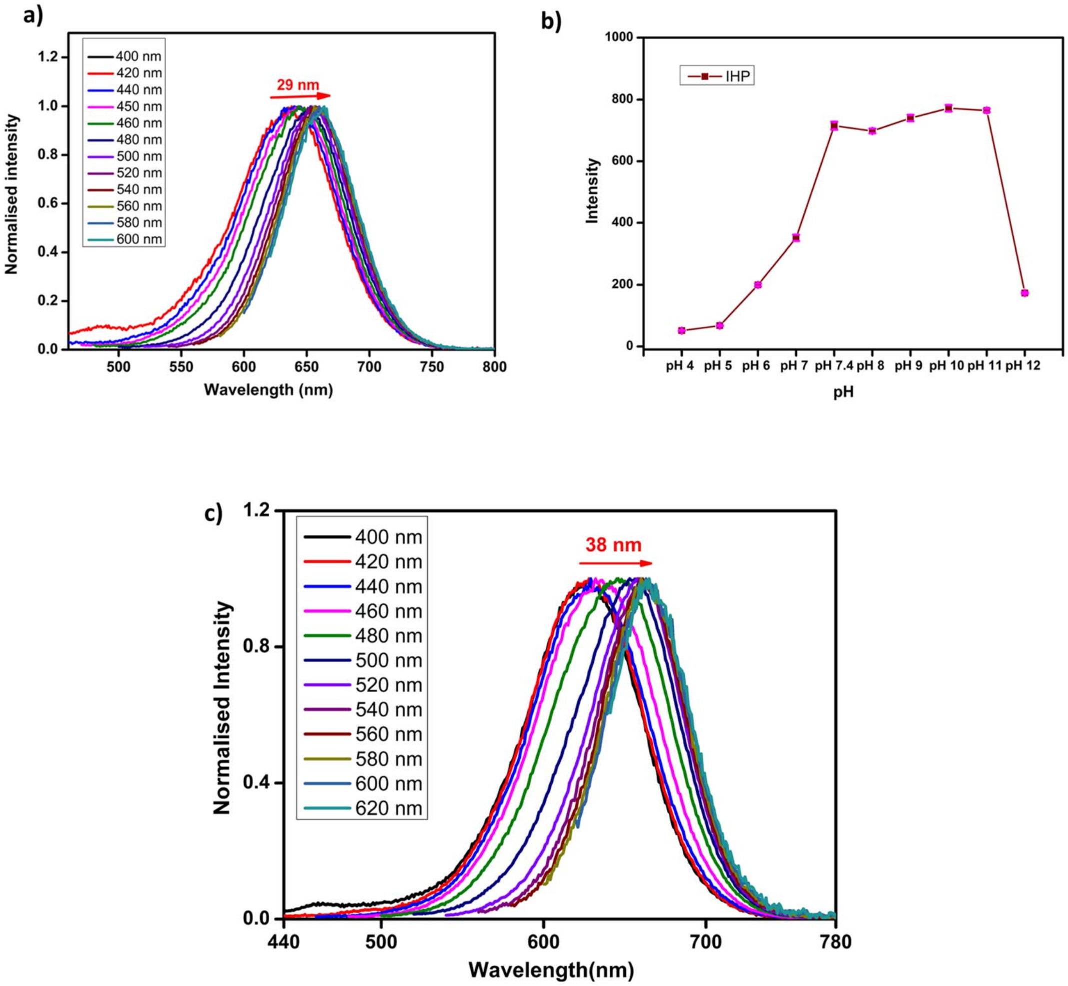

Fig. 3 (a) Normalised emission spectra IHP in DMSO : H_2O (1 : 1) recorded at different excitation wavelengths (b) the emission intensity of IHP at 635 nm at different pH (c) normalised emission spectra IHP in DMSO : H_2O (1 : 1) recorded at different excitation wavelengths after adjusting the pH to 7.4.

conducted experiments to record the emission spectra of IHP in DMSO:PBS at various pH levels ranging from 4 to 9 (Fig. 3b). The observations revealed a decrease in the emission of IHP under acidic conditions. This can be attributed to the conversion of the pyridine moiety in IHP to pyridinium ion in acidic pH, rendering it water-soluble.[59] Hence, this transformation prevents aggregation and, consequently, diminishes the emission of IHP in acidic environments. As the pH is made alkaline, the emission maximum intensity increases up to pH 10. A dramatic increase in intensity is observed from pH 7 to 8, potentially explaining the lower magnitude of the red-shift emission intensity in water (pH 7) as compared to the PBS buffer (10 mM, pH 7.4). The emission intensity is almost same from pH 8 to pH 10 and based on that we could say that IHP can be useful in physiological conditions. Then IHP was taken in DMSO : H_2O (1 : 1), where the pH was adjusted to pH 7.4 and the emission spectra was recorded by increasing the excitation wavelength in the red-edge of the spectra and then found that the magnitude of the red-shift (38 nm) was almost equal to the magnitude of the shift in DMSO:PBS (Fig. 3c). All these results proved that IHP forms J-aggregate in DMSO : PBS (10 mM, pH 7.4, 1 : 1). Similar pattern of absorption and emission was observed when IHP was studied in different DMSO : H_2O ratios. This confirms the AIE behaviour of IHP.

3.3 Sensing studies

With our aim to utilize IHP for $ONOO^-$ and considering the alkaline-dependent stability of $ONOO^-$,[60] extensive experimentation with various buffer solutions was conducted, ultimately leading to the selection of PBS buffer (10 mM, pH 7.4) for spectral studies. All the sensing studies were done in DMSO : PBS (10 mM, pH 7.4, 1 : 1) system due to the alkaline stability of $ONOO^-$.

3.3.1 Detection of $ONOO^-$. The stock solution of IHP was made to 0.001 M in DMSO. Based on the literature the analytes were prepared to 0.01 M concentration in water.[9,61] The sensing potential of the IHP (10 μM) was evaluated in DMSO : PBS buffer in a 1 : 1 ratio (10 mM, pH = 7.4) in the presence of $ONOO^-$ (50 μM). As shown in Fig. S18,† the absorption spectra of IHP showed two distinct bands at 435 nm and 540 nm. Upon the addition of $ONOO^-$, these absorption bands shifted to 460 nm, which was accompanied by a noticeable colour change as shown in the insets of Fig. S18a,† enabling the colorimetric sensing of $ONOO^-$.

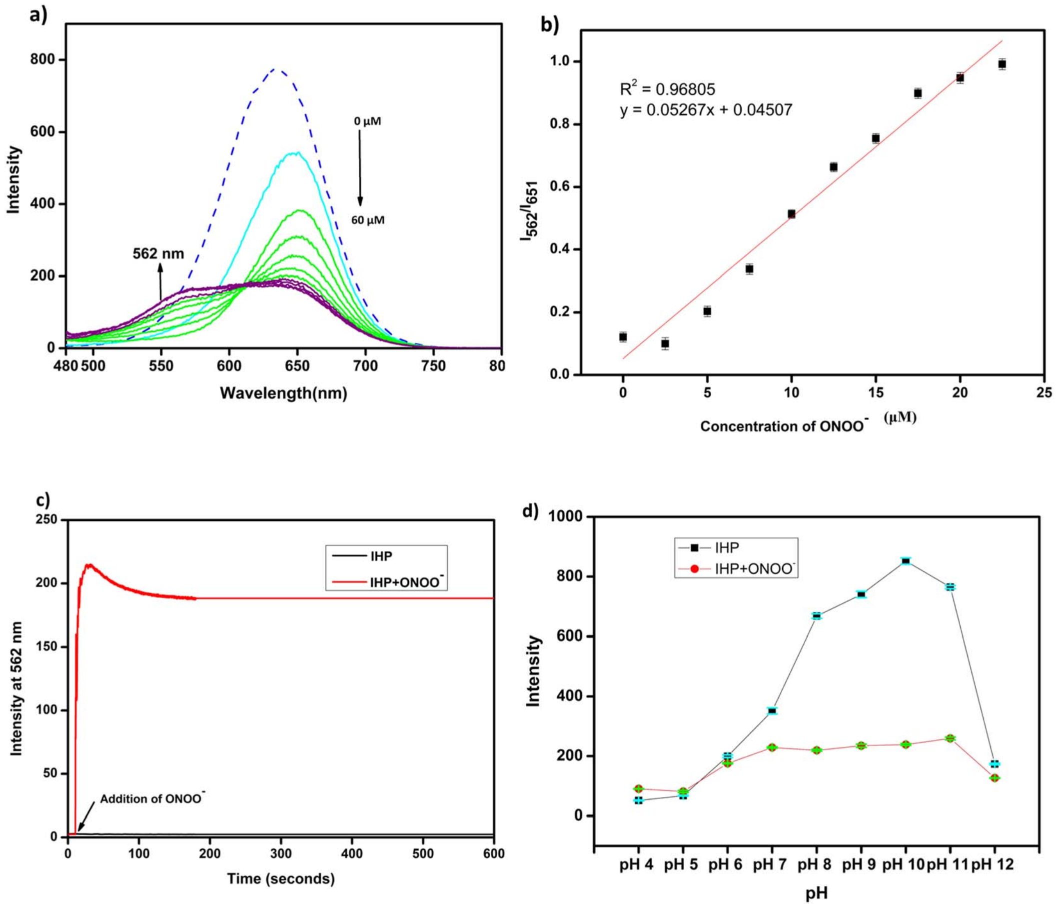

Fig. 4 (a) Fluorescence emission of IHP in DMSO : PBS (1 : 1, v/v, pH 7.4) on incremental addition of $ONOO^-$ [the dashed line represents the emission of IHP in DMSO : PBS (1 : 1, v/v, pH 7.4) without the addition of $ONOO^-$] (b) linear plot between fluorescence intensity at 651 nm and concentration of $ONOO^-$ (c) time response graph of IHP in DMSO : PBS (1 : 1, v/v, pH 7.4) with $ONOO^-$ and (d) the effect of pH study on IHP and IHP + $ONOO^-$ in DMSO : PBS (1 : 1, v/v, pH 7.4).

Initially, IHP when excited at 460 nm displayed a strong fluorescence emission at 635 nm. However, the addition of $ONOO^-$ resulted in the reduction of fluorescence intensity of IHP and a blue shift in the emission maximum to 562 nm with reduced intensity. This change in behaviour was also marked by the change in fluorescence emission from red to orange as depicted in Fig. S18b.† The large Stoke's shift (~100 nm) observed can prevent it from autofluorescence and thus helps in bioimaging applications.

3.3.2 Quantitative detection of $ONOO^-$. To evaluate the selective binding efficiency of IHP with $ONOO^-$, a fluorescence titration experiment was conducted by incrementally increasing the concentration of $ONOO^-$. As shown in Fig. 4a, the reaction between IHP and $ONOO^-$ resulted in two distinct emission bands at 651 nm and 562 nm. The initial emission peak of IHP at 635 nm exhibited a slight red shift to 651 nm, with its intensity decreasing as the $ONOO^-$ concentration increased. Concurrently, a blue-shifted emission band at 562 nm emerged and grew in intensity corresponds to the emission of compound **3**. Hence, the observed emission changes in IHP upon interaction with $ONOO^-$ are ascribed to the formation of de-aggregated species and the production of compound **3**. Compound **3** is an ESIPT emissive molecule,[49] but the blue-shifted peak appears to be of lower intensity, possibly due to insufficient excitation energy at the chosen wavelength.

A plot between concentration of $ONOO^-$ against fluorescence intensity at I_{562}/I_{651} (Fig. 4b) exhibited a linear relationship with linear coefficient ($R^2 = 0.97$). The detection limit was calculated using $3\sigma/m$, where σ is the standard deviation of the blank, obtained by running the blank sample ten times, and m is the slope of the plot obtained. The LOD was found to be 1.1 μM. The above experimental data showed that the probe IHP can detect $ONOO^-$ even in its low concentration.

3.3.3 Kinetics study. The kinetics analysis of the probe aimed to determine the time required to detect $ONOO^-$. To achieve this, the fluorescence intensity of both IHP and IHP with $ONOO^-$ was monitored as a function of time as depicted in Fig. 4c. Initially, the fluorescence emission of IHP (10 μM) at 562 nm remained stable for a duration of 30 minutes. With $ONOO^-$ (50 μM), the fluorescence intensity began to increase gradually. This increase continued until it reached a stable level after approximately 200 seconds. These results demonstrate the stability of IHP and its ability to rapidly identify $ONOO^-$.

3.3.4 The pH effect. Given the physiological pH of approximately 7.4, it was crucial to evaluate the impact of pH on IHP's fluorescence response to $ONOO^-$. At acidic pH levels, IHP exhibited weak or no fluorescence due to the conversion of its pyridine moiety into a pyridinium ion. This transformation increased its water solubility, preventing aggregation and, consequently, low fluorescence emission. However, as the pH became more alkaline, aggregation began to occur, enabling the probe to emit fluorescence. The results, depicted in Fig. 4d, indicate that the probe's functionality remained largely stable across the physiological pH range of 7 to 11. These findings underscore the probe's strong potential for biological applications, demonstrating its reliability and effectiveness under relevant physiological conditions. Furthermore, the fluorescence emission of IHP after reacting with $ONOO^-$ remained nearly unchanged, with only minor variations. This consistency can be attributed to the formation of compound **3**, whose structure is pH-stable and retains consistent electronic properties across the tested pH range.

3.3.5 Selectivity and interference studies. To detect $ONOO^-$ in physiological environments, it is crucial for the probe to selectively identify $ONOO^-$ without interference from other similar analytes. Therefore, a selectivity and interference experiment were conducted to evaluate the ability of the sensor IHP (10 μM) to recognize $ONOO^-$. The sensing potential of IHP was tested against a range of comparable analytes, including metal ions (Al^{3+}, Ca^{2+},Co^{2+}, Cu^+, Cu^{2+}, Fe^{2+}, Fe^{3+}, Mg^{2+}, Na^+, K^+, Zn^{2+}), anions (F^-, Br^-, I^-, CO_3^{2-}, HCO_3^-, NO_2^-, NO_3^-, SCN^-, $S_2O_3^{2-}$, SO_3^{2-}, SO_4^{2-}, OCl^-) and reactive oxygen and sulphur species (H_2O_2, OH, TBHP, $^1O_2$, NO, HNO, $ONOO^-$).

As illustrated in the fluorescence selectivity graph of IHP with various analytes (Fig. S19a†), no changes in the emission of IHP was seen, even on the addition of 100 μM of these similar analytes, except for $ONOO^-$ (50 μM). These spectral studies confirm the high selectivity of IHP for $ONOO^-$ ions in a DMSO : PBS (1 : 1) solution.

To further assess the resistance of IHP to interference, the emission at 635 nm was measured in the presence of other active species at higher concentrations along with $ONOO^-$

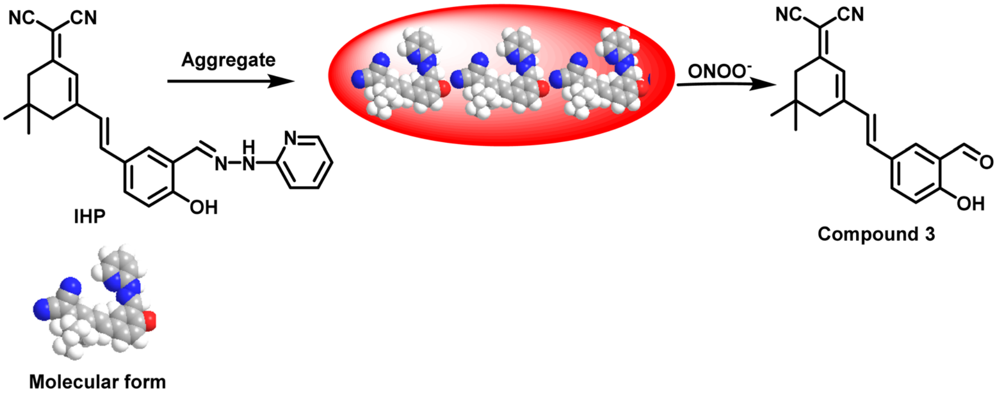

Scheme 2 Sensing mechanism of IHP with $ONOO^-$.

(Fig. S19b†). From the experimental results, it was observed that only a small portion of these substances interfered with the probe's response to ONOO$^-$. Several factors may explain this outcome. Firstly, the probe's selectivity plays a crucial role in minimizing interference, as it is specifically designed to interact with the unique chemical structure of ONOO$^-$. The probe may also exhibit kinetic preference, reacting more rapidly with ONOO$^-$ than with other similar analytes, allowing it to produce a detectable signal for ONOO$^-$ while remaining unaffected by other substances. Additionally, the chemical properties of ONOO$^-$ contribute to the observed specificity. As a short-lived and highly reactive species, ONOO$^-$ can interact with the probe before less reactive analytes can do so. Furthermore, the pH dependence of ONOO$^-$ stability is a key factor. Since ONOO$^-$ is stable only within a specific pH range, probes and assays are often optimized for this condition, reducing interference from other analytes that may be less stable or reactive in the same environment. These factors collectively explain why only a limited number of substances interfered with the probe's response to ONOO$^-$, featuring its potential suitability for detecting ONOO$^-$ in complex environments. This robust selectivity and interference resistance highlight IHP's effectiveness as a fluorescent sensor for peroxynitrite in physiological conditions.

3.3.6 Sensing mechanism. IHP, due to its C=N isomerization of the hydrazone moiety, is expected to be weakly or non-fluorescent. However, based on its AIE characteristics, IHP exhibits strong red emission. Upon the addition of ONOO$^-$, an oxidative cleavage of the C=N bond occurs, leading to a deprotection reaction that produces compound **3** (Scheme 2). Compound **3** demonstrates ESIPT behaviour and is emissive. The observed shift in emission maxima is attributed to the formation of de-aggregated species and compound **3**. Compared to IHP, the emission maximum of compound **3** is blue shifted, validating the transition from red to orange emission. The blue-shifted peak appears less intense, potentially due to insufficient excitation energy at the chosen wavelength or because compound **3** is inherently less emissive compared to the aggregates of IHP under the conditions used for sensing studies.

To verify the above mechanism, the reaction between IHP and ONOO$^-$ was monitored using ^{1}H NMR. As seen in Fig. S20,† IHP had a sharp singlet at $\delta = 8.34$ ppm, which correspond to the –CH=N– group. However, on addition of ONOO$^-$, the sharp singlet at $\delta = 8.34$ ppm disappeared and two peaks at δ 10.25 ppm and 11.02 ppm appears which correspond to the –CHO and –OH proton in compound **3** respectively. The mechanism was further confirmed by HRMS in which the mass observed 319.1441 matched with the calculated mass of compound **3** (Fig. S21†).

3.3.6.1 Theoretical calculations. To investigate the sensing mechanism and solvent behaviour of IHP, theoretical calculations were conducted using Density Functional Theory (DFT) with the B3LYP/6-31G basis set. Time-Dependent DFT (TDDFT) analysis revealed that in IHP, the electron cloud in the Highest Occupied Molecular Orbital (HOMO) is distributed across the molecule, with a significant concentration on the hydrazinyl pyridine moiety. In contrast, the Lowest Unoccupied Molecular Orbital (LUMO) shows electron density predominantly localized on the electron-deficient dicyanoisophorone moiety (Fig. 5).

Upon the addition of ONOO$^-$, IHP is converted to compound **3**, wherein the electron densities in both HOMO and LUMO are uniformly distributed throughout the molecule which supports the ICT behaviour. The HOMO–LUMO energy gap of IHP is smaller compared to compound **3**, aligning with the observed blue shift in the absorption and emission spectra of the probe and its complex with ONOO$^-$.

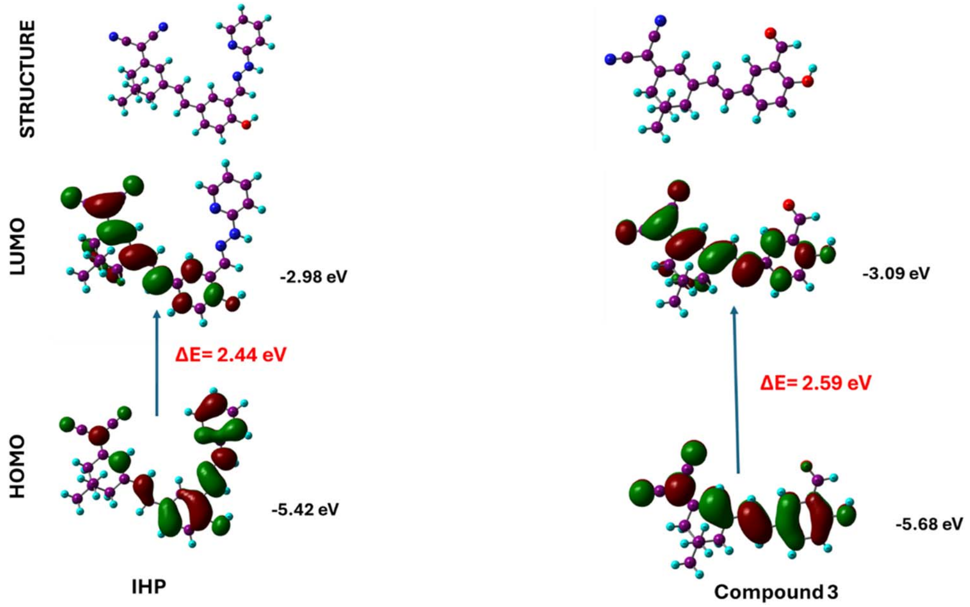

Fig. 5 Theoretical data estimated by DFT calculations to support the sensing mechanism.

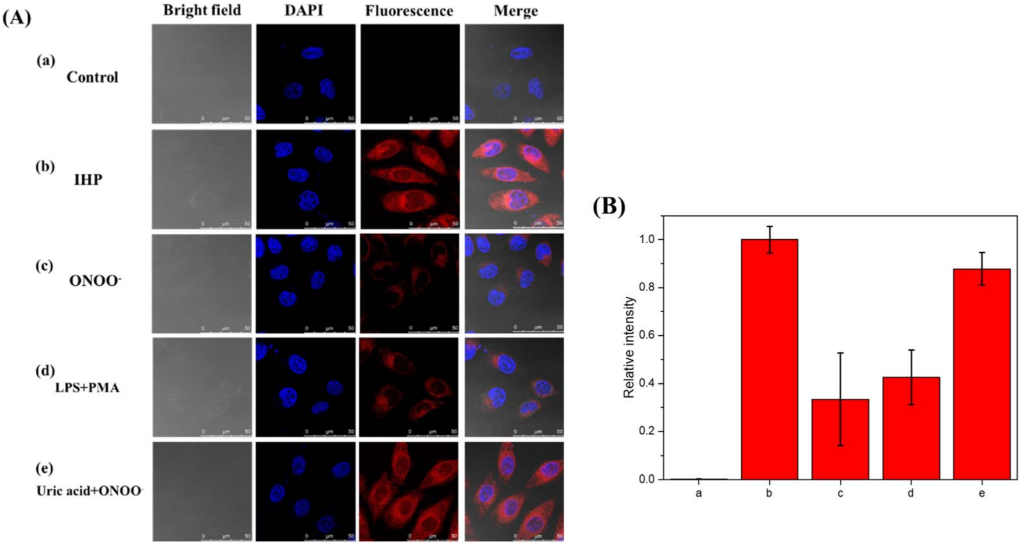

Fig. 6 (A) Confocal images of HeLa cells: (a) control group; (b) HeLa cells were pre-loaded IHP (10 μM) at 37 °C for 20 minutes; the cells then treated with (c) $ONOO^-$ (50 μM), (d) LPS (1 μg mL^{-1}) PMA (10 nM) and (e) co-incubated with $ONOO^-$ (50 μM) and uric acid (200 μM). (B) Relative intensity from fluorescence images in (A). The relative intensity from fluorescence image in (b) is defined as 1.0. Blue fluorescence: $\lambda_{ex} = 405$ nm, $\lambda_{em} = 435–485$ nm. Red fluorescence: $\lambda_{ex} = 555$ nm, $\lambda_{em} = 620–700$ nm. Each experiment was repeated thrice, and error bars are included.

3.3.7 Bioimaging. HeLa cells were used to monitor the bioimaging ability of IHP exogenously and endogenously. The imaging studies were carried out in PBS buffer. The control group of cells showed no intracellular fluorescence (Fig. 6). The cells loaded with 10 μM IHP and incubated for twenty minutes at 37 °C showed bright red fluorescence. The cells were treated with $ONOO^-$ (50 μM), resulting in a reduction in red fluorescence intensity. However, the fluorescence was not completely quenched, supporting the observed shift in emission from red to orange. This indicates that IHP can detect exogenous $ONOO^-$. To monitor the endogenous $ONOO^-$ by IHP, the cells loaded with IHP were treated with lipopolysaccharide (LPS, 1 μg mL^{-1}) and phorbol 12-myristate 13-acetate (PMA, 10 nM) for another 30 minutes. It was found weak red fluorescence emission. Uric acid (200 μM), a $ONOO^-$ scavenger was co-incubated with $ONOO^-$ (50 μM) and found that the intensity of the bright red emission increased. These results suggest that IHP can trace both exogenous and endogenous $ONOO^-$.

4. Conclusion

A donor–acceptor-based fluorescent probe was designed by integrating 2-hydrazinyl pyridine with a dicyanoisophorone fluorophore to specifically detect peroxynitrite ($ONOO^-$). Leveraging the AIE characteristics, the probe exhibited excitation-dependent fluorescence changes, highlighting the presence of multiple emission species. A red shift in emission further indicated the formation of J-aggregates. The synthesized probe demonstrated several advantageous properties for $ONOO^-$ detection, including a pronounced fluorescence response, high selectivity, and strong anti-interference capability against structurally similar analytes. These results were attributed to the incorporation of a strategically designed hydrazone functional group. Additionally, the probe was effective across the physiological pH range and exhibited low cytotoxicity, enabling the visualization of both exogenous and endogenous $ONOO^-$ in living cells. A fluorescent probe exploiting the AIE behaviour was developed was developed that offer robust and precise detection of peroxynitrite ($ONOO^-$) in both biological and environmental systems.

Data availability

The data supporting this article have been included as part of the ESI.†

Author contributions

Raguraman Lalitha: conceptualization, methodology, investigation, writing – original draft, review and editing. Vivek Vishnu Halnor: investigation, conceptualization, methodology. Yueh-Hsun Lu: investigation, conceptualization, methodology. Shu Pao Wu: visualisation, investigation, resources. Sivan Velmathi: resources, supervision, writing – review and editing, validation.

Conflicts of interest

The authors state that "there are no conflicts to declare".

Acknowledgements

The author (R. Lalitha, File Number 09/895(0015)/2020-EMR-I) is grateful to the Council of Scientific and Industrial Research – HRDG for the financial support.

References

1 J. Sun, X. Cao, W. Lu, Y. Wei, L. Kong, W. Chen, X. Shao and Y. Wang, *Theranostics*, 2023, **13**, 1716–1744.
2 Z. Chen, S. Zhang, X. Li and H. wang Ai, *Cell Chem. Biol.*, 2021, **28**, 1542–1553.
3 C. Liu, X. Zhang, Z. Li, Y. Chen, Z. Zhuang, P. Jia, H. Zhu, Y. Yu, B. Zhu and W. Sheng, *J. Agric. Food Chem.*, 2019, **67**, 6407–6413.
4 Q. An, S. Su, L. Chai, Y. Wang, X. Wang, X. Li, T. Liang, W. Hu, X. Song and C. Li, *Talanta*, 2023, **253**, 124073.
5 X. Sun, K. Lacina, E. C. Ramsamy, S. E. Flower, J. S. Fossey, X. Qian, E. V. Anslyn, S. D. Bull and T. D. James, *Chem. Sci.*, 2015, **6**, 2963–2967.
6 Y. Fu, H. Nie, R. Zhang, F. Xin, Y. Tian, J. Jing and X. Zhang, *RSC Adv.*, 2018, **8**, 1826–1832.
7 J. Lu, Z. Li, Q. Gao, J. Tan, Z. Sun, L. Chen and J. You, *Anal. Chem.*, 2021, **93**, 3426–3435.
8 M. Zhu, H. Zhou, D. Ji, G. Li, F. Wang, D. Song, B. Deng, C. Li and R. Qiao, *Dyes Pigments*, 2019, **168**, 77–83.
9 Y. Zhang and D. Ma, *Spectrochim. Acta, Part A*, 2021, **244**, 1–5.
10 Z. Wang, W. Wang, P. Wang, X. Song, Z. Mao and Z. Liu, *Anal. Chem.*, 2021, **93**, 3035–3041.
11 Z. Li, J. Lu, Q. Pang and J. You, *Analyst*, 2021, **146**, 5204–5211.
12 C. Sun, W. Du, P. Wang, Y. Wu, B. Wang, J. Wang and W. Xie, *Biochem. Biophys. Res. Commun.*, 2017, **494**, 518–525.
13 J. Zhang, Y. Li, J. Zhao and W. Guo, *Sens. Actuators, B*, 2016, **237**, 67–74.
14 Z. Liu, S. Mo, Z. Hao and L. Hu, *Int. J. Mol. Sci.*, 2023, **24**(16), 12821.
15 S. Xu, K. C. Yan, Z. H. Xu, Y. Wang and T. D. James, *Chem. Soc. Rev.*, 2024, **53**, 7590–7631.
16 M. Zhou, Y. Lin, T. Bai, T. Ye, Y. Zeng, L. Li, Z. Qian, L. Guo, H. Liu and J. Wang, *Sens. Actuators, B*, 2024, **414**, 135994.
17 Y. Shen, X. Zhang, Y. Zhang, H. Li and Y. Chen, *Sens. Actuators, B*, 2018, **258**, 544–549.
18 Y. Shen, X. Zhang, Y. Zhang, Y. Wu, C. Zhang, Y. Chen, J. Jin and H. Li, *Sens. Actuators, B*, 2018, **255**, 42–48.
19 Khadija, H. Irshad, S. Rafique, A. M. Khan, S. Nawazish, H. ur Rehman, M. Imran, S. A. Shahzad and U. Farooq, *Spectrochim. Acta, Part A*, 2023, **290**, 122273.
20 R. X. Zhang, P. F. Li, W. J. Zhang, N. Li and N. Zhao, *J. Mater. Chem. C*, 2016, **4**, 10479–10485.
21 G. J. Mao, G. Q. Gao, W. P. Dong, Q. Q. Wang, Y. Y. Wang, Y. Li, L. Su and G. Zhang, *Talanta*, 2021, **221**, 121607.
22 S. Kim, C. W. Ko, T. Lim, S. Yoo, H. J. Ham, S. Y. Kang, S. Kang, S. K. Cho and M. S. Han, *Dyes Pigments*, 2019, **171**, 107762.
23 R. F. Khairutdinov and N. Serpone, *J. Phys. Chem. B*, 1997, **101**, 2602–2610.
24 J. L. Bricks, Y. L. Slominskii, I. D. Panas and A. P. Demchenko, *Methods Appl. Fluoresc.*, 2017, **6**, 012001.
25 P. Mahato, S. Saha, S. Choudhury and A. Das, *Chem. Commun.*, 2011, **47**, 11074–11076.
26 F. Xu, T. T. Testoff, L. Wang and X. Zhou, *Molecules*, 2020, **25**, 4478.
27 J. Heo, D. P. Murale, H. Y. Yoon, V. Arun, S. Choi, E. Kim, J. S. Lee and S. Kim, *Aggregate*, 2022, **3**, 1–35.
28 S. Hussain, H. Muhammad Junaid, M. Tahir Waseem, W. Rauf, A. Jabbar Shaikh and S. Anjum Shahzad, *Spectrochim. Acta, Part A*, 2022, **272**, 121021.
29 K. Mukherjee, T. I. Chio, H. Gu, A. Banerjee, A. M. Sorrentino, D. L. Sackett and S. L. Bane, *ACS Sens.*, 2017, **2**, 128–134.
30 P. Das, A. Kumar, A. Chowdhury and P. S. Mukherjee, *ACS Omega*, 2018, **3**, 13757–13771.
31 Y. Zhou, H. Xu, Q. X. Li, Z. R. Hou, Y. W. Wang and Y. Peng, *Org. Biomol. Chem.*, 2023, **21**, 1270–1274.
32 M. Zhang, J. Li, L. Yu, X. Wang and M. Bai, *RSC Adv.*, 2020, **10**, 14520–14524.
33 Q. Hu, Q. Huang, K. Liang, Y. Wang, Y. Mao, Q. Yin and H. Wang, *Dyes Pigments*, 2020, **176**, 108229.
34 H. Sun, X. X. Tang, R. Zhang, W. H. Sun, B. X. Miao, Y. Zhao and Z. H. Ni, *Dyes Pigments*, 2020, **174**, 108051.
35 G. Jiang, C. Li, Q. Lai, X. Liu, Q. Chen, P. Zhang, J. Wang and B. Z. Tang, *Sens. Actuators, B*, 2021, **329**, 129223.
36 J. Li, J. Tang, X. Yang, P. Xie, J. Liu, D. Zhang and Y. Ye, *Sens. Actuators, B*, 2022, **358**, 131513.
37 Z. Wang, J. Gong, P. Wang, J. Xiong, F. Zhang and Z. Mao, *Talanta*, 2023, **252**, 123811.
38 X. Han, X. Yang, Y. Zhang, Z. Li, W. Cao, D. Zhang and Y. Ye, *Sens. Actuators, B*, 2020, **321**, 128510.
39 H. Xie, J. Zhang, C. Chen, F. Sun, H. Liu, X. He, K. W. K. Lam, Z. Li, J. W. Y. Lam, G. Q. Zhang, D. Ding, R. T. K. Kwok and B. Z. Tang, *Mater. Chem. Front.*, 2021, **5**, 1830–1835.
40 B. Guo, W. Shu, W. Liu, H. Wang, S. Xing, J. Chen and X. Zhang, *Sens. Actuators, B*, 2021, **344**, 130206.
41 M. Li, H. Han, S. Song, S. Shuang and C. Dong, *Spectrochim. Acta, Part A*, 2021, **261**, 120044.
42 Y. Shen, M. Li, M. Yang, Y. Zhang, H. Li and X. Zhang, *Spectrochim. Acta, Part A*, 2019, **222**, 117230.
43 Y. Dong, Y. Yang, Y. Tao, M. Fang, C. Li and W. Zhu, *J. Fluoresc.*, 2024, DOI: **10.1007/s10895-024-03961-w**.
44 X. F. Hou, Y. L. Xue, J. G. Yang, Z. S. Li, Z. H. Xu, W. Li and L. Yuan, *Anal. Chem.*, 2024, **96**(44), 17657–17664.
45 X. Hou, Y. Xue, C. Liu, Z. Li and Z. Xu, *Spectrochim. Acta, Part A*, 2024, **320**, 124665.
46 J. Wu, Y. Lin, Y. Yu, Y. Li, T. Ye, H. Zhou, L. Li and J. Wang, *Dyes Pigments*, 2022, **206**, 110597.
47 L. Zhong, H. Niu, Y. Lin, T. Ye, S. Zheng, K. Chen, L. Li, L. Guo and J. Wang, *Microchem. J.*, 2024, **206**, 111540.
48 Y. Shen, X. Zhang, Y. Zhang, H. Li, L. Dai, X. Peng, Z. Peng and Y. Xie, *Anal. Chim. Acta*, 2018, **1014**, 71–76.
49 F. Huo, Y. Zhang, Y. Yue, J. Chao, Y. Zhang and C. Yin, *Dyes Pigments*, 2017, **143**, 270–275.
50 J. Harathi and K. Thenmozhi, *Mater. Chem. Front.*, 2020, **4**, 1471–1482.
51 A. Jose, A. Tharayil and M. Porel, *Polym. Chem.*, 2023, **14**, 3309–3316.
52 Y. Meng, X. Yao, K. Zhong, Y. Li and L. Tang, *Eur. J. Org. Chem.*, 2023, **26**(18), e202300022.
53 C. Xia and Y. Qian, *New J. Chem.*, 2016, **40**, 144–150.

54 T. T. Trang, T. T. H. Pham, N. Van Dang, P. T. Nga, M. Van Linh and X. H. Vu, *RSC Adv.*, 2024, **14**, 9538–9546.
55 Y. Kong, R. Wu, X. Wang, G. Qin, F. Wu, C. Wang, M. Chen, N. Wang, Q. Wang and D. Cao, *RSC Adv.*, 2022, **12**, 27933–27939.
56 P. Verma and H. Pal, *J. Phys. Chem. A*, 2014, **118**, 6950–6964.
57 N. H. Mudliar, P. M. Dongre and P. K. Singh, *Sens. Actuators, B*, 2019, **301**, 127089.
58 A. Samanta, *J. Phys. Chem. B*, 2006, **110**, 13704–13716.
59 V. D. Singh, R. S. Singh, R. P. Paitandi, B. K. Dwivedi, B. Maiti and D. S. Pandey, *J. Phys. Chem. C*, 2018, **122**, 5178–5187.
60 T. Hou, K. Zhang, X. Kang, X. Guo, L. Du, X. Chen, L. Yu, J. Yue, H. Ge, Y. Liu, A. M. Asiri, K. A. Alamry, H. Yu and S. Wang, *Talanta*, 2019, **196**, 345–351.
61 L. Yuan, W. Lin, S. Zhao, W. Gao, B. Chen, L. He and S. Zhu, *J. Am. Chem. Soc.*, 2012, **134**, 13510–13523.